Article

The Microchip Laser and Its Drive Control System for Planetary Mass Spectrometry Measurements

Wenbo Liu [1,2], Peng Sang [2], Yang Cao [2], Yaning Liu [2], Huan Wang [1,2] and Baoquan Li [1,2,*]

[1] School of Astronomy and Space Science, University of Chinese Academy of Sciences, Beijing 100049, China; liuwenbo21@mails.ucas.ac.cn (W.L.); wanghuan20@mails.ucas.ac.cn (H.W.)

[2] Laboratory of Advanced Measurement Technology, National Space Science Center, Chinese Academy of Sciences, Beijing 100190, China; sangp@nssc.ac.cn (P.S.); caoyang@nssc.ac.cn (Y.C.); liuyaning@nssc.ac.cn (Y.L.)

[*] Correspondence: lbq@nssc.ac.cn

Featured Application: The microchip laser and its driver control system designed in this study possess the characteristics of being lightweight, compact, and low power consumption. It serves as a fitting candidate for planetary mass spectrometry missions, particularly as a micro-focusing excitation light source for Time-of-Flight (TOF) mass spectrometers. The output laser wavelength is 1064 nm, with pulse duration as low as 410 ps, a continuously adjustable frequency range from 100 to 1000 Hz, a minimum focal spot size of 15 μm, and a single pulse energy reaching up to 16.8 μJ. Additionally, the overall weight is only 106 g. This microchip laser allows for adjustable focal length, spot size, and laser power output, making it versatile for tasks such as compositional analysis and in-situ dating in deep space exploration. Additionally, it can serve as a portable device for mineral exploration and non-destructive testing, presenting extensive application prospects in the field of mass spectrometry analysis.

Abstract: To fulfill the requisites of planetary mass spectrometry applications, this paper introduces the creation of a miniaturized, low-power passive Q-switched microchip laser system. The entire system, inclusive of the laser and all electronic components, weighs 106 g, with power consumption below 3 W. The laser output exhibits a pulse duration of 410 ps, accompanied by a single pulse energy of 16.8 μJ. Augmented by the optical focusing system, the system attains a focal spot size of approximately 15 μm and laser irradiance of up to 22 GW/cm^2. The driving control system facilitates versatile regulation of parameters such as output current amplitude, pulse duration, and frequency, thereby modulating the laser output frequency and duty cycle. The microchip laser fully meets the power requirements for exciting plasma from planetary rocks and soil.

Keywords: microchip laser; passively Q-switched; TOF mass spectrometry; planetary mass spectrometry

1. Introduction

Mass spectrometry technology has extensive applications in planetary exploration, particularly Laser Ablation Time-of-Flight Mass Spectrometry (LA-TOF-MS), which has garnered significant attention as one of the most effective methods for measuring isotopes and conducting compositional analysis [1–4]. By using a microchip laser, sample material is ablated and ionized shot by shot. Charged species enter the mass analyzer and in the field-free drift path, they separate in time according to their mass-to-charge ratios. By measuring the time sequence of detector signals, the composition of substances in the sample can be accurately determined [5]. This advanced measurement technique provides unique insights, enabling a deeper understanding of the composition and structure of planets and other celestial bodies, thus driving forward our exploration of the universe.

Compared to other mass spectrometry instruments such as Sector Field Mass Spectrometers and Quadrupole Mass Spectrometers, LA-TOF-MS offers advantages such as

wide mass range, high sensitivity, fast response time, and simple structure [6]. These benefits are particularly advantageous for exploration missions involving most planets and satellites, including asteroids, comets, and moons [7]. According to results published in the literature, this new type of mass spectrometer achieves a mass resolution exceeding 500, with detection limits reaching the parts per billion (ppb) level, and it requires minimal resources [8], making it more suitable for the development needs of deep space exploration. In comparison to Laser-Induced Breakdown Spectroscopy (LIBS) systems already deployed in space, Laser Ablation TOF Mass Spectrometry offers higher sensitivity and resolution, capable of detecting trace elements in samples and providing precise quantification and in-depth analysis capabilities [9].

The technology was previously detailed by Rohner et al., who devised a prototype LA-TOF-MS and conducted laboratory assessments. Their system weighed a mere 500 g, occupied a volume of 650 cm^3, and operated at an average power of 3 W [10,11]. It employed custom microchip lasers from Poly-Scientific as the excitation source, with parameters delineated in Table 1. Experimental findings indicated that under these parameters, the microchip laser adeptly induced sample plasma, and in conjunction with TOF-MS, achieved adequate mass resolution to distinctly discriminate neighboring isotopes. LA-TOF-MS technique was also designed for application in the "Forbes-Soil" Mars rover, wherein the LA-TOF-MS onboard is anticipated to attain elemental and isotopic analysis accuracy levels of at least 10% and 1%, respectively, alongside the capability to precisely localize samples and conduct layer-by-layer analyses to a depth of 10 μm [12]. However, unfortunately, due to mission failure, it was unable to demonstrate its capabilities in planetary mass spectrometry. Despite the high-power output of the accompanying microchip laser in their system, it features a low repetition rate and large pulse duration, necessitating the utilization of a laser radiation attenuator and neutral optical filter to diminish laser energy during operational phases. Furthermore, there are currently some advanced technologies still under development. For example, Wurz et al. at the University of Bern are soon to introduce the CLPS-LIMS system, which aims to achieve better spectral analysis capabilities using a 532 nm laser wavelength [13].

Table 1. Literature research.

Literature	Wavelength	Pulse Duration	Spot Size	Single Pulse Energy	Frequency	Weight	Power
[10,11]	1064 nm	0.66 ns	15 μm	12 μJ	7 kHz	500 g (whole system)	3 W
[12]	1064 nm	7 ns	30 μm	15 mJ	0.1 Hz	2.7 kg (whole system)	8 W
[13]	532 nm	1.4 ns	30 μm	40 μJ	0.1 kHz	Weight was not provided, but length 100 mm and width 34 mm	-
This paper	1064 nm	0.41 ns	15 μm	16.7 μJ	0.1 k–1 kHz Adjustable	106 g	3 W

In LA-TOF-MS, the performance of the microchip laser as the excitation device is crucial, directly impacting the accuracy and efficiency of mass spectrometry measurements. This paper aims to meet the increased demands of planetary mass spectrometry on microchip lasers by developing a superior-performance microchip laser. Compared to existing literature, this microchip laser has a smaller weight and volume: the prototype's mass is only 106 g (including the laser and all electronic components), with a low overall power consumption of less than 3 W. Additionally, the laser produced by this microchip laser exhibits better beam quality, with output energy and spot size better suited for directly exciting samples to generate plasma [14]. The laser's pulse duration is as low as 410 ps, with a single-pulse energy of 16.8 μJ, and it is equipped with an optical focusing system

to achieve micro-focused laser output. At a focal length of 30 mm, representing near field focusing, the spot size is 15 μm, while also providing a solution for adjusting the output power. These superior performance characteristics make this microchip laser an ideal choice for planetary mass spectrometry, providing a more precise and efficient tool for planetary science research.

2. Materials and Methods

Earlier studies suggest that achieving laser irradiance on the target in TOF mass spectrometry at the order of 1 GW/cm^2 is necessary to generate a plasma plume with minimal elemental fractionation, reflecting the surface's true composition [15]. To attain such high irradiance states from dense solids, lasers equipped with short-pulse passive Q-switching systems are required, offering advantages in coupling with the time-of-flight mass analyzer [16]. Given the stringent mass and power budget constraints in deep space exploration missions, the microchip laser adopts a design strategy utilizing semiconductor laser-pumped passive Q-switching. In contrast to conventional lasers, the microchip laser's resonant cavity is notably short, resulting in a brief photon lifetime and facilitating the generation of short pulses lasting on the order of nanoseconds or sub-nanoseconds. Passive Q-switching eliminates the need for electronic switching devices, reducing the system's size and complexity while enhancing power efficiency. The repetition frequency can surpass a kilohertz, and the single-pulse energy can reach tens of microjoules. In addition, such systems provide excellent pulse to pulse energy stability, which is of high importance for laser ablation techniques. This approach addresses the unique challenges posed by deep space exploration missions, ensuring efficient and precise performance of the LA-TOF-MS under the constraints of limited mass and power resources.

The operating principle of the microchip laser, designed for application in deep space exploration TOF mass spectrometers, revolves around employing a short-cavity resonant structure with a saturable absorber to regulate laser generation. Initially, the saturable absorber exhibits a high absorption coefficient, which gradually decreases as the optical intensity rises. Upon reaching the saturation intensity, the saturable absorber swiftly transitions to a transparent state, facilitating the generation of a robust pulsed laser output [17]. Contrasted with continuous pumping, pulsed pumping notably mitigates thermal effects on the crystal, resulting in improved pulse output energy, beam quality, and pulse stability. This paper aims to offer an introduction to the microchip laser, encompassing both structural and electronic design perspectives.

2.1. Structural Design of Microchip Laser

Illustrated in Figure 1, a semiconductor laser diode (LD) serves as the initial energy source. The energy is coupled to the laser crystal through a lens assembly, functioning as an imaging optical system. The laser crystal comprises a solid gain medium and a saturable absorber, wherein the saturable absorber passively adjusts the quality factor (Q) to emit laser pulses with a narrow bandwidth and high energy. Typically, when the Q value is high, cavity loss is low. Thus, during the pumping phase, electrons transfer to the upper energy level. At this juncture, due to the characteristics of the saturable absorber, the Q value inside the cavity is low, resulting in high losses, preventing laser formation and retaining the electrons in the upper energy level. Once a sufficient number of electrons accumulate in the upper energy level, the Q value experiences a rapid increase. Subsequently, the electrons undergo a swift transition to the lower energy level, resulting in an instantaneous high-power laser output. This operational principle highlights the role of the saturable absorber in passive Q adjustment and the dynamic electron transitions that lead to precise and controlled pulsed laser emissions in deep space exploration TOF mass spectrometers.
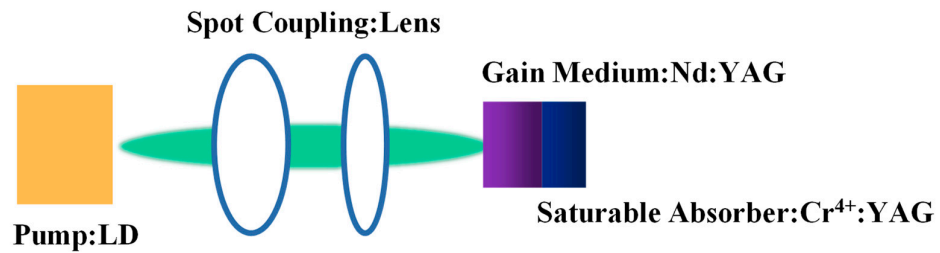
Figure 1. Illustration of a passively Q-switched microchip laser.

Considering the imperative for small size, low power consumption, and a compact structure, the chosen pumping source is a semiconductor laser with a maximum power of 10 W and a wavelength of 808 nm. It possesses a threshold current of 1.8 A and operates at a voltage below 2.2 V. The advantageous low current emission requirement facilitates the development of a low-power drive system. To ensure optimal conversion efficiency, end-pumping is implemented, aligning the pump light co-linearly with the resonant cavity. Significant overlap between the pumped volume and the TEM_{00} mode enhances efficient energy transfer. Utilizing an imaging optical system, the pump light is collimated and focused, effectively suppressing optical distortions. The distribution of pump light aligns with the volume of the resonant cavity mode, ensuring precise incidence within the laser crystal, as depicted in Figure 2. This meticulous design approach contributes to the microchip laser's efficiency, addressing the specific demands of deep space exploration missions for a compact, low-power laser system with optimal performance.
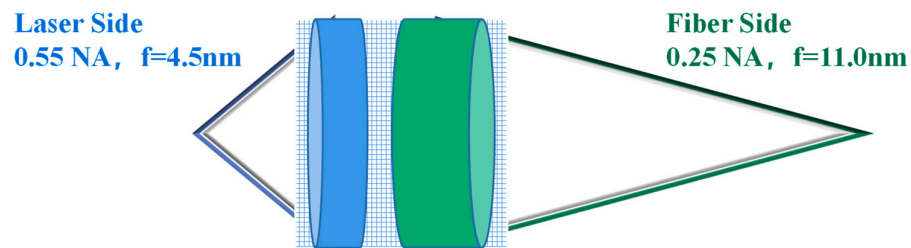

Figure 2. Schematic of imaging optical system of LD pumped laser.

The conventional approach to preparing laser crystals involves various methods, such as bonding Nd^{3+}:YAG gain media to saturable absorbing crystals, including Cr^{4+}:YAG [18]. Alternatively, one material can be grown on the other to form a composite crystal [19], or a saturable absorbing material can be coated onto the gain medium [20]. The composite structure comprising Nd^{3+}:YAG and Cr^{4+}:YAG is characterized by its simplicity, good thermal stability, and extended service life, rendering it a high-quality passive Q-switched laser crystal [21]. To leverage the absorption characteristics of Cr^{4+}:YAG at 1 μm, meticulous polishing of two planes perpendicular to the optical axis is necessary during production. The pumping-side surface requires coating with a dielectric material to facilitate pump light transmission and exhibit high reflectivity at the oscillation wavelength, ensuring the efficient absorption of pump light and the effective operation of the laser crystal at the desired wavelength. This methodical preparation enhances the performance and reliability of the laser crystal, making it a valuable component for passive Q-switching in laser systems.

Leveraging the operational characteristics of the semiconductor laser and laser crystal, a meticulously designed microchip laser structure that meets the specified requirements has been crafted, as shown in Figure 3. The pumping source and laser crystal find their place on a baseplate crafted from oxygen-free copper, serving for collimation and alignment while facilitating rapid temperature conduction. At the central part of the baseplate, a cavity is hollowed to accommodate a lens assembly. This non-heating component minimizes contact with the baseplate, reducing the system's heat dissipation area and consequently lowering

heat dissipation power consumption. The laser crystal is securely pressed onto the baseplate through two L-shaped structures, enveloped by indium foils to ensure efficient heat conduction. Small holes are incorporated into the baseplate to house negative temperature coefficient thermistors, enabling real-time monitoring of the microchip laser's operating temperature. Additionally, a groove is integrated into the bottom of the laser housing to accommodate a semiconductor cooler, allowing temperature control of the entire working environment and ensuring the stable operation of the microchip laser. A protective window is designed at the laser's emission port, using a flat mirror to isolate dust and moisture from the surroundings. This comprehensive design approach addresses thermal management challenges, ensuring the microchip laser's reliable and efficient performance in deep space exploration environments.
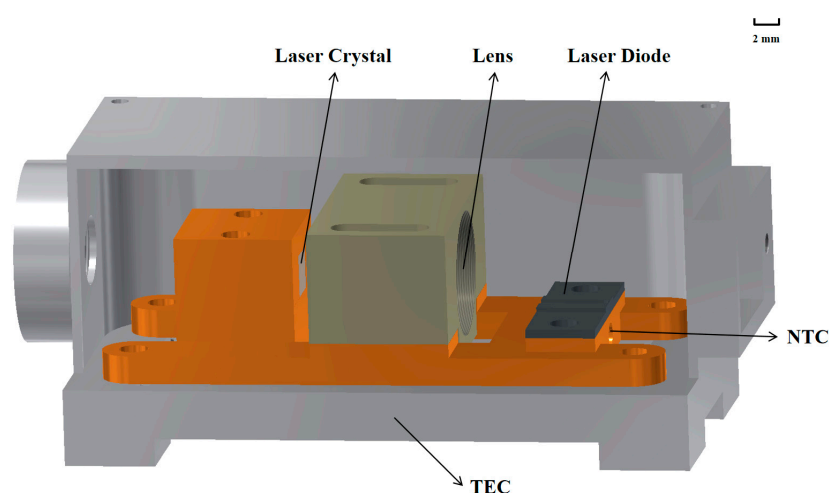

Figure 3. Structural diagram of microchip laser.

As indicated in existing literature, an increase in spot size, under the same laser power density, results in a heightened spatial charge of the resulting ion beam. Considering the limited drift length in subsequent mass analyzers, this could compromise ion focusing, leading to a notable decrease in mass resolution [22]. To ensure precise excitation of the test substance, yielding singly charged ions for subsequent TOF mass spectrometry testing [23], configuring a power adjustment device becomes imperative. This device facilitates simple adjustment of the output power during testing. Consequently, to attain micro-focus laser output and streamline the adjustment of the laser's output power, an optical focusing system has been meticulously designed for the laser in this study. Illustrated in Figure 4, the optical focusing system incorporates a removable optical sleeve, providing adaptability for different application needs. The system employs optical lenses with varying refractive indices to expand and contract, aiding in minimizing the spot size, increasing the focal length, and achieving micro-focus output. A $\lambda/2$ waveplate and a polarizing beamsplitter (PBS) collaborate to form a variable power attenuator, enabling power adjustment within the 5% to 95% range. Tuning the waveplate allows for precise adjustment of the laser intensity output. Concurrently, a portion of the signal light can be redirected for synchronous detection. This integrated optical focusing system enhances the precision and versatility of the microchip laser for optimal performance in diverse testing environments.
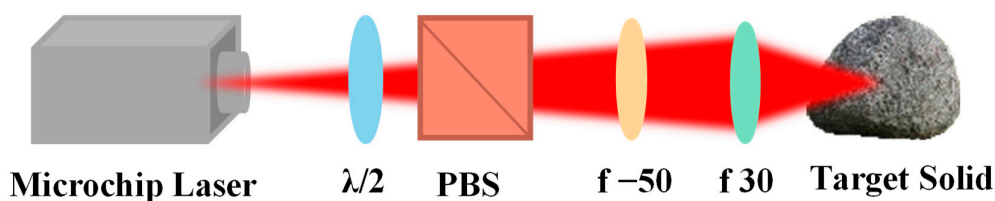

Figure 4. Design diagram of the optical focusing system.

2.2. Design of Drive and Control System

Due to the strict constraints on available space and power in deep space exploration missions, all electronic systems in microchip lasers suitable for planetary mass spectrometry measurements must be customized. The laser operates based on the principle of current injection, inducing particle inversion in the active region. The recombination of electrons in the conduction band and holes in the valence band in semiconductor materials results in stimulated emission, converting electrical energy into optical energy excitation [24]. Therefore, beyond the impact of the structure itself, the stability of the output from the electronic driving system is crucial for the laser's performance. The stability and ripple of the driving current for the semiconductor laser used as a pumping source can alter the optical power, central wavelength, and spectral linewidth of the emitted pump light. For an ideal pump laser, the linewidth should be narrow, the central wavelength stable, and it should have an appropriate photon intensity. This necessitates high stability of the driving current and minimal ripple. Additionally, lasers are highly sensitive to temperature variations. Every 1 °C fluctuation can lead to approximately 0.2–0.3 nm variation in the pump source's wavelength, accompanied by a noticeable decrease in the lifespan [25]. Therefore, the temperature control accuracy should be less than 0.1 °C. To mitigate thermal effects during laser operation while meeting low-power usage conditions, this study adopts a controlled constant current source for pulse output. This tailored electronic design ensures optimal performance and reliability of the microchip laser in the challenging conditions of deep space exploration.

The electronic driving system comprises a control unit, a pulse constant current source system, a temperature control system, and a protection circuit. The overall structure is shown in Figure 5. The control circuit generates a reference signal, feeding it to the pulse constant current source system and the temperature control system to produce the required current based on the settings. It also engages in communication with the upper computer to monitor the laser's operational status in real-time. The pulse constant current source circuit operates to generate controlled and stable pulse current, facilitating proper laser operation. Simultaneously, the temperature control system upholds the microchip laser's operation under specified temperature conditions. The protection circuit is intricately designed to avert damage to the laser in the event of sudden system issues or abnormal conditions, ensuring the laser's safety and longevity.
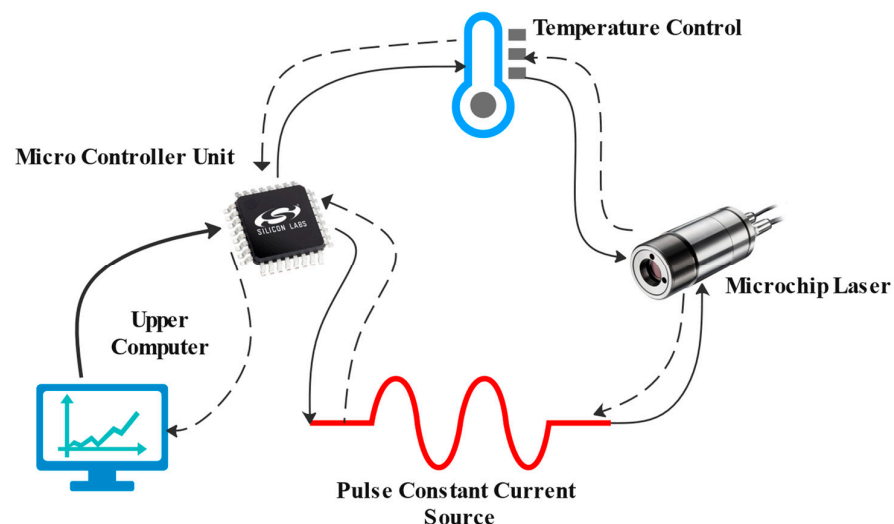

Figure 5. Overall Structure Diagram of Laser Driver System.

The control unit is equipped with a high-level anti-radiation microcontroller, and its structure is illustrated in Figure 6. Leveraging the built-in PCA (Pulse-Code Modulation) and DAC0 (Digital-to-Analog Converter), it governs the amplitude, frequency, and duty cycle of the output current. The synthesized reference signal is dispatched to the subsequent

pulse constant current source system through analog switches, allowing users to adjust the parameters of the output current based on different application scenarios for the laser. DAC1 provides a reference voltage to the temperature control system, facilitating temperature regulation. Two ADC (Analogl-to-Digita Converter) channels are employed to collect parameters related to current and temperature, which are then conveyed to the upper computer for display. This sophisticated control unit design ensures precise and flexible control of the microchip laser, adapting to various operational requirements in deep space exploration missions.
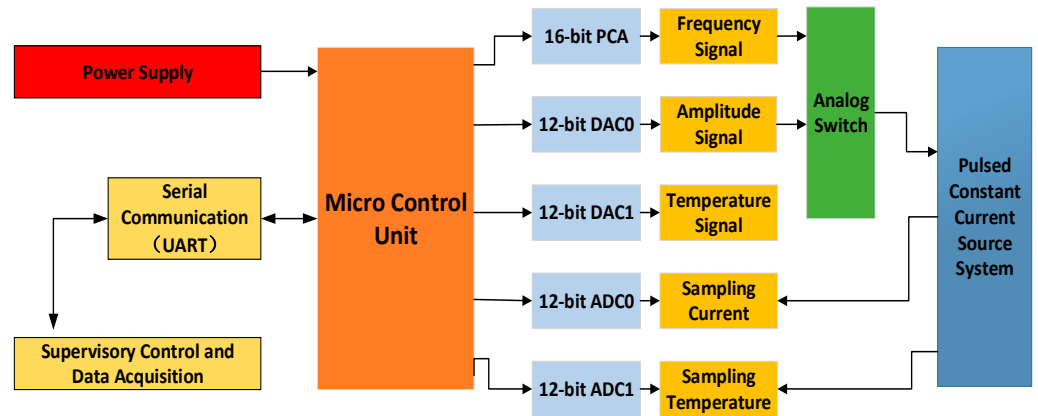

Figure 6. Control Circuit Structure Diagram.

The pulse constant current source system is depicted in Figure 7, and its operational workflow is approximately as follows: Initially, as the control unit provides the reference signal, the driving voltage (V_G) starts to increase gradually from zero. When it exceeds the threshold voltage (V_{th}), the drain current of the MOSFET begins to appear, and simultaneously, the load current (I_L) is generated. As V_G increases, I_L also gradually increases until the current reaches the rated value as required by the reference signal, as detected by the current-sensing resistor. Afterward, the system continuously regulates the current to meet the requirements of the reference signal. This dynamic control mechanism ensures precise and stable pulse current output for optimal performance of the microchip laser in various operational scenarios.
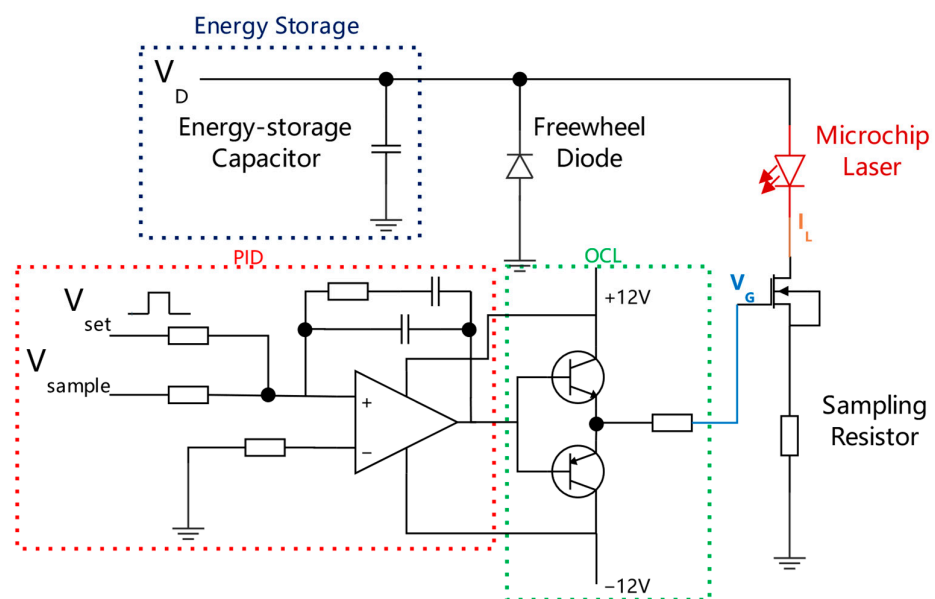

Figure 7. Schematic Diagram of Control Circuit.

The drive for the laser necessitates a sufficiently short rise time of a large current, a challenge that conventional DC-DC converters find difficult to address directly. Therefore, an energy storage system is selected as the implementation scheme to store energy, leveraging the discharge characteristics of a capacitor to supply instantaneous current. This approach not only fulfills the requirements of driving the laser but also alleviates the demands on the transient power of the external power source, meeting power limitations in deep space exploration applications. To maintain a minimal voltage drop across the laser terminals during operation, it is typically required that the voltage drop of the energy storage capacitor does not exceed 10% during discharge. According to

$$C_{\min} = \frac{I_{\max} t_{on}}{\Delta u} \tag{1}$$

the required capacitance value can be calculated. Here, $I_{\max}$ represents the required current, t_{on} is the pulse duration of the current, and Δu is the permissible voltage drop across the energy storage capacitor.

The core of the pulse constant current source system lies in the Metal-Oxide-Semiconductor Field-Effect Transistor (MOSFET). Its operation in the linear region is harnessed to control the drain current by manipulating the gate voltage. In this configuration, the current exhibits constant characteristics, and the MOSFET responds rapidly to changes in the gate voltage. Moreover, it demonstrates good linearity in response to gate voltage variations, facilitating precise control of the output current. Since the MOSFET operates in the linear region, it needs to endure a certain voltage drop. It is crucial to ensure that it consistently operates within the Forward Biased Safe Operation Area. Additionally, when operating in the saturation region, devices with lower ON resistance should be chosen to minimize power dissipation on the MOSFET.

Due to the short duration of the pulse current during laser operation, a high bandwidth requirement exists for the driving system. Consequently, the pulse constant current source system employs analog loop compensation, offering a larger bandwidth compared to digital loop compensation. To enhance the accuracy and stability of the pulse current, a proportional-integral-derivative (PID) control algorithm is employed to regulate the system. It adjusts the system's response speed through the proportional and integral terms, enabling it to respond more rapidly to changes in the input signal and adapt to the requirements of high-bandwidth short-pulse applications. Additionally, the derivative term suppresses system oscillations, ensuring stability and smooth operation. Following Formula (2) below, K_p represents proportional gain, $\frac{K_p}{T_r}$ represents integral time constant, and $K_p\tau$ represents derivative time constant. The compensating network incorporates a system compensating poles and zeros. It provides a high gain in the low-frequency range, enhancing the open-loop gain of the system, while rapidly attenuating the loop gain in the high-frequency range. In practical adjustment, it is advisable to start by adjusting the proportional coefficient from the middle toward both ends. Subsequently, incrementally increase the integral coefficient and derivative coefficient from zero until a smooth response curve is observed, indicating that the laser driver has entered the desired operational state. This sophisticated control strategy ensures precise and efficient pulse current delivery, meeting the demanding requirements of laser operation in deep space exploration missions.

$$y(t) = K_p x(t) + \frac{K_p}{T_r} \int_0^t x(t) + K_p \tau \frac{dx(t)}{dt} \tag{2}$$

To achieve fast turn-on and turn-off of the MOSFET, shortening the rising and falling edges of the pulse current, gate current is required for the gate-source and gate-drain capacitance to charge and discharge. However, the operational amplifier's drive capability is limited. Therefore, an Output Capacitor-Less (OCL) circuit is introduced after PID control in the pulse constant current source to enhance the drive capability of the MOSFET.

For the temperature control system, high-grade integrated temperature control chips are selected to achieve a balance between temperature control accuracy, low power consumption, and compact design. These chips offer high integration, small size, high precision, and excellent safety. The control diagram is illustrated in Figure 8. Utilizing its internally stabilized zero-crossing wave operational amplifier and integral amplifier, it forms a PID regulation system. One input terminal imports the voltage value for the set temperature from the microcontroller's DAC through a bridge circuit, while the other input terminal is connected to a Negative Temperature Coefficient Thermistor (NTC) to collect the real-time voltage value corresponding to the temperature. After processing by the PID controller, the driving current for controlling the Thermoelectric Cooler (TEC) is provided through a Field Effect Transistor (FET). To ensure the cooling efficiency and longevity of the laser, a high-quality semiconductor cooler was selected. It features 71 pairs of thermoelectric couples and has dimensions of $31.3 \times 17.6 \times 3$ mm^3, matching the area of the oxygen-free copper baseplate in the laser system, thereby minimizing heat dissipation power consumption.
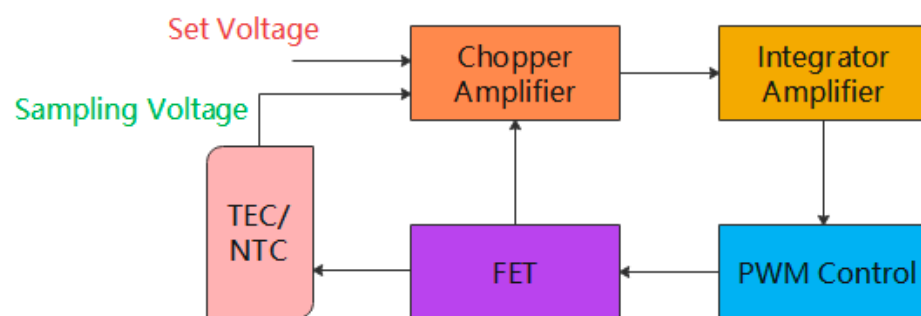

Figure 8. Structure diagram of temperature control system.

3. Experiments and Indicator Testing

The laser and its associated electronics were assembled into a compact physical unit, as depicted in Figure 9. Following assembly, the laser weighs merely 46 g, occupying dimensions of $48 \times 22 \times 22$ mm^3, while the driving control electronics section weighs 60 g, with dimensions measuring $62 \times 42 \times 22$ mm^3. Power supply and control can be conveniently established by connecting through a miniature aviation connector. The paper experimented and tested the relevant parameters of the laser. It should be noted that the currently assembled laser is a prototype for functional verification. In actual space science experiments, targeted adjustments may be necessary based on specific usage environments, and the parameters may vary accordingly.
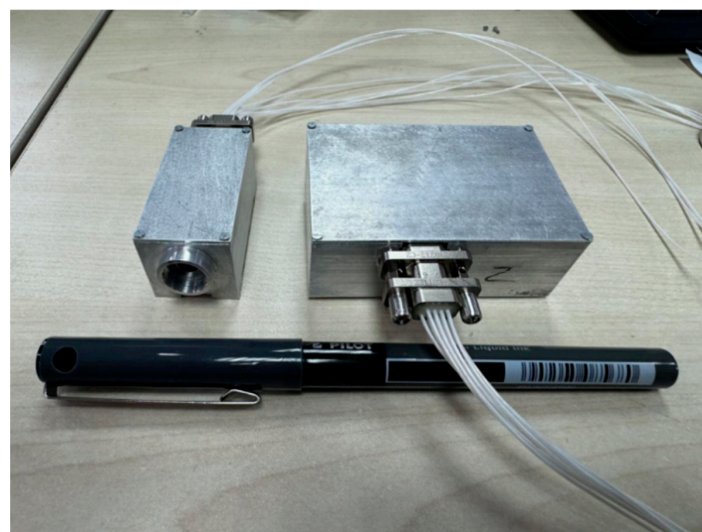

Figure 9. Photograph of microchip laser.

Figure 10 illustrates the output waveform of the developed microchip laser driver electronics. Sending commands from the upper computer to the control system, set the parameters of the output current to a frequency of 500 Hz, a pulse duration of 150 μs, and an amplitude of 5 A. Post-processing by the MCU results in the generation of a reference signal, and the current waveform is observed to be stable with rise and fall times less than 10 μs, displaying no significant overshoot or undershoot. At this juncture, convenient adjustments to the pump source's current frequency, for increasing or decreasing the microchip laser's repetition rate, can be executed through commands dispatched from the upper computer. Furthermore, parameters such as amplitude and pulse duration of the output current, along with the system's operating temperature, can be easily modified as required.
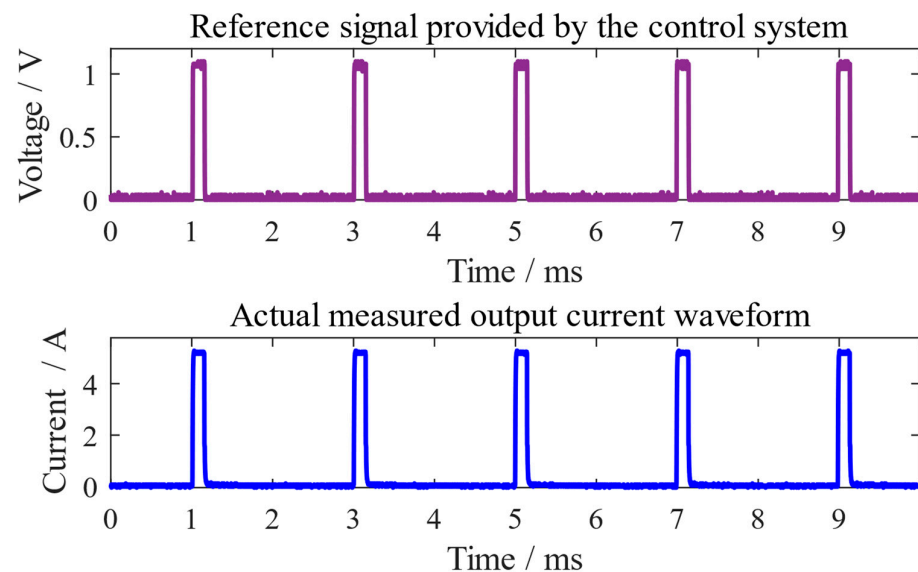

Figure 10. Experimentally measured current waveform plot.

Assessing the temperature control system's performance entailed configuring various temperature gradients. The experiment is conducted at room temperature, approximately 23 °C. Following a 5-s delay, an infrared thermometer was employed to gauge the temperature of the laser's operating panel. The results, detailed in Table 2, demonstrate that the working environment promptly responds to temperature control signals, ensuring a consistently stable operating temperature. This validation underscores the reliability and effectiveness of the temperature control system in maintaining the desired thermal conditions during the operation of the microchip laser.

Table 2. Operation test of the temperature control system.

Set Temperature (°C)	Actual Measured Temperature (°C)	Deviation Value (°C)	Overall Power Consumption (W)
15	15.1	+0.1	3.3
18	18.2	+0.2	3.1
21	20.9	−0.1	2.8
24	24.0	0	2.7
27	27.1	+0.1	2.9
30	29.8	−0.2	3.0

Collaborating with the laser, we fine-tuned the optimal working conditions. Setting the operating temperature at 25 °C and the operating current at 5 A, the tested laser output is illustrated in Figure 11. At this juncture, the laser pulse duration measured 410 ps, and each input electrical pulse precisely corresponded to an actual output laser pulse without any stray pulses. This observation affirms that the temperature and current settings were

appropriate, ensuring the laser crystal operated under suitable conditions. The overall power consumption of the system at this point was less than 3 W. It is important to note that the overall power consumption of the system is dependent on the operating environment of the microchip laser. From a power distribution perspective, the current required to drive the microchip laser accounts for approximately 1.5 W. Additionally, the temperature control system operates at around 1–1.5 W power consumption when working at temperatures between 20–30 °C.
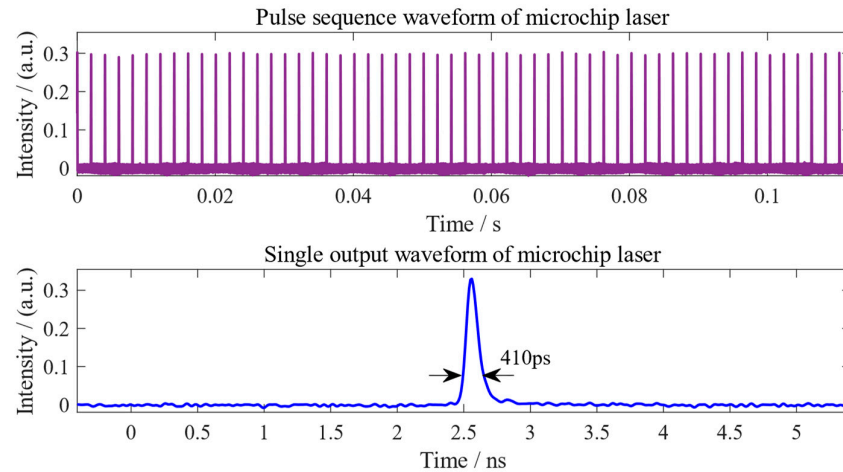

Figure 11. Laser output waveform plot.

The stability of the laser output was assessed using a laser power probe, as depicted in Figure 12. The single-pulse energy measured approximately 16.8 μJ, and the laser power stability, quantified by the QMS value, exhibited a 0.3% variation over 5 min. Although this study did not conduct extended tests on the laser's operational lifetime, calculations considering continuous operation time and pulse frequency suggest that the laser can maintain stability for up to 150,000 working pulses. The output power fluctuation remains below 0.5%, satisfying the requirements for testing in conjunction with the TOF mass spectrometer. Subsequent tests on the laser's operational lifetime will be conducted during actual operations in the future. This meticulous evaluation provides confidence in the laser's stability and performance under varying operational conditions.
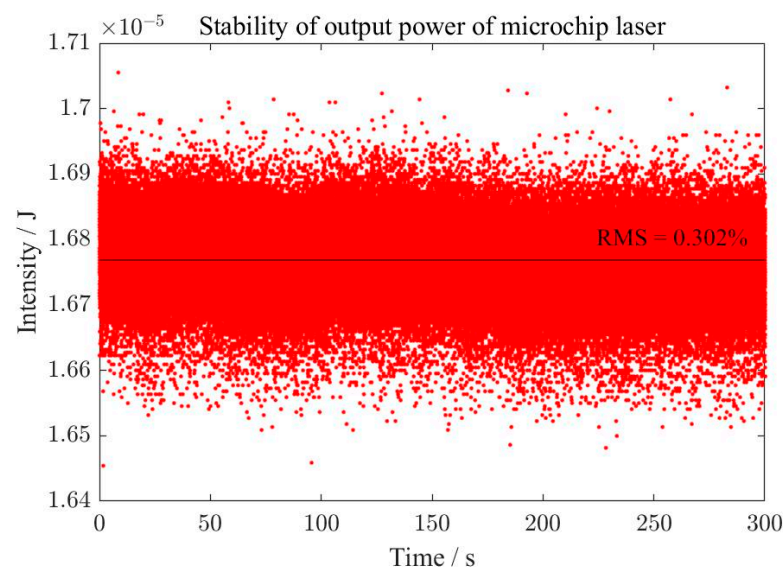

Figure 12. Power stability testing under single pulse output conditions.

As shown in Figure 13, we verified the stability of the initial pulse. Within 30 s of starting power supply, the laser output power fluctuated slightly. This was due to the reaction time of the temperature control system. After 30 s, the laser power stabilized at 16.8 μJ, and the initial fluctuation amplitude was less than 2%.
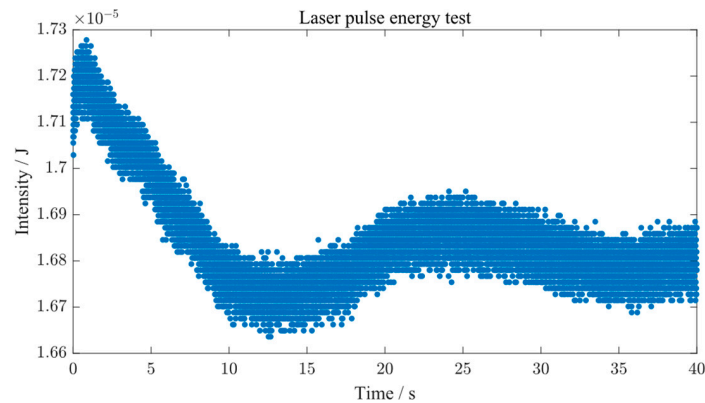

Figure 13. Initial laser pulse energy stability test.

We utilized a CCD detector to test the output spot of the microchip laser, revealing an effective diameter of approximately 15 μm and the beam quality was M^2 = 1.4, as shown in Figure 14. This paper employs the Thorlabs C230220P visual optical system. In future research, we will design optical pathways that are better suited for the internal structure of microchip lasers, aiming to minimize distortion and improve beam quality.
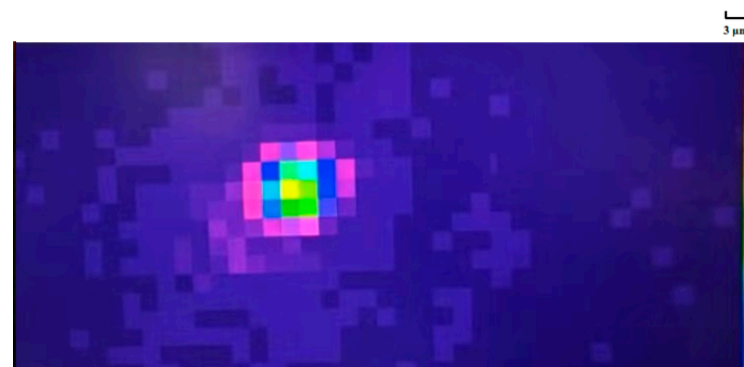

Figure 14. The image depicting the laser spot output tested with a CCD detector.

Subsequently, the microchip laser was tested in conjunction with the designed optical focusing system, as shown in Figure 15. According to the approach adopted in this paper, with a designed focal length of 30 mm, white light was observed on the surface of the sample where it was excited, confirming the generation of plasma on the solid surface. In practical use, the optimal laser focus point can be determined by assessing the brightness of white light. Moreover, the half-wave plate could be adjusted to obtain laser outputs at different powers.

To further confirm that the designed microchip laser can excite samples to generate plasma, we used a frequency of 500 Hz to excite the sample for 5 s, generating 2500 laser pulses with an energy of 16.8 μJ each. The post-excited aluminum foil sample was then observed under a microscope, as shown in Figure 16. It can be seen that there are noticeable impact craters on the foil, with a diameter of approximately 15 μm, matching the size of the microchip laser's focal spot.

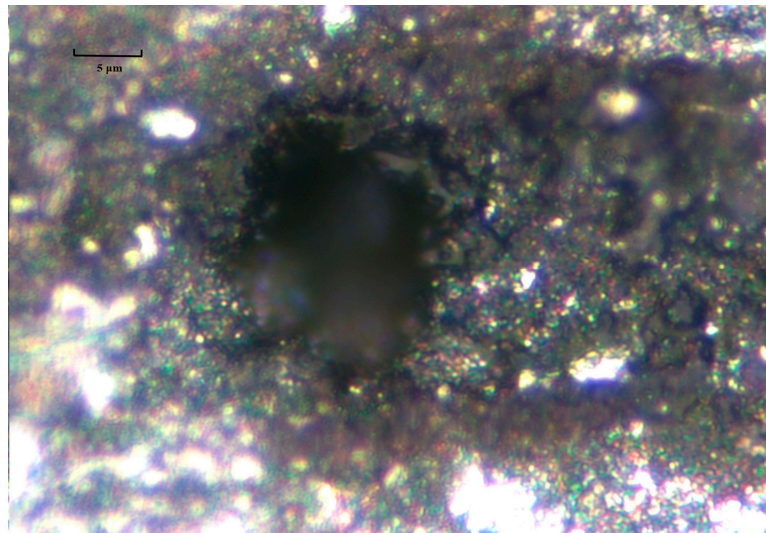**Figure 15.** Laser excitation of microchip laser for the generation of plasma in stone.

Figure 16. The impact craters on the aluminum foil generated by laser irradiation observed under a microscope.

4. Conclusions

In summary, the microchip laser developed in this paper emits the laser with a wavelength of 1064 nm, pulse duration of 410 ps, and single pulse energy of 16.8 μJ. The accompanying electronic drive system allows for continuous adjustment of the operating frequency between 100–1000 Hz and temperature control precision of ±0.1 °C. The total power consumption of the entire system, including all electronic components, is less than 3 W. This microchip laser serves as a miniaturized, high-power plasma excitation source for deep space exploration TOF mass spectrometers. In subsequent work, it will be integrated and jointly tested with the TOF mass spectrometer currently under development. TOF mass spectrometers are characterized by their lightweight, compact, and low-power nature, making them suitable for onboard component analysis in planetary exploration missions and as portable devices for mineral resource exploration, thus offering broad application prospects.

Author Contributions: Conceptualization, W.L. and B.L.; methodology, W.L.; software, Y.L. and P.S.; validation, H.W., W.L. and Y.C.; formal analysis, W.L.; investigation, P.S.; resources, Y.L.; data curation, H.W.; writing—original draft preparation, W.L.; writing—review and editing, Y.C.; visualization, Y.C.; supervision, B.L.; project administration, W.L.; funding acquisition, B.L. All authors have read and agreed to the published version of the manuscript.

Institutional Review Board Statement: Not applicable.

Informed Consent Statement: Not applicable.

Data Availability Statement: The data presented in this study are available in the article.

Conflicts of Interest: The authors declare no conflict of interest.

References

1. Chou, L.; Mahaffy, P.; Trainer, M.; Eigenbrode, J.; Arevalo, R.; Brinckerhoff, W.; Getty, S.; Grefenstette, N.; Da Poian, V.; Fricke, G.M. Planetary mass spectrometry for agnostic life detection in the Solar System. *Front. Astron. Space Sci.* **2021**, *8*, 755100. [CrossRef]
2. Managadze, G.; Safronova, A.; Luchnikov, K.; Vorobyova, E.; Duxbury, N.; Wurz, P.; Managadze, N.; Chumikov, A.; Khamizov, R.K. A new method and mass-spectrometric instrument for extraterrestrial microbial life detection using the elemental composition analyses of Martian regolith and permafrost/ice. *Astrobiology* **2017**, *17*, 448–458. [CrossRef] [PubMed]
3. Riedo, A.; Bieler, A.; Neuland, M.; Tulej, M.; Wurz, P. Performance evaluation of a miniature laser ablation time-of-flight mass spectrometer designed for in situ investigations in planetary space research. *J. Mass Spectrom.* **2013**, *48*, 1–15. [CrossRef] [PubMed]
4. Huang, Z.; Tan, G.; Zhou, Z.; Chen, L.; Cheng, L.; Jin, D.; Tan, X.; Xie, C.; Li, L.; Dong, J. Development of a miniature time-of-flight mass/charge spectrometer for ion beam source analyzing. *Int. J. Mass Spectrom.* **2015**, *379*, 60–64. [CrossRef]
5. Ramisetty, R. A New Time-Of-Flight Mass Spectrometer (TOF-MS) for Noble Gas Analysis. Ph.D. Thesis, Universität Bern, Bern, Switzerland, 2015.
6. Ren, Z.; Guo, M.; Cheng, Y.; Wang, Y.; Sun, W.; Zhang, H.; Dong, M.; Li, G. A review of the development and application of space miniature mass spectrometers. *Vacuum* **2018**, *155*, 108–117. [CrossRef]
7. Li, X.; Brinckerhoff, W.; Managadze, G.; Pugel, D.; Corrigan, C.; Doty, J. Laser ablation mass spectrometer (LAMS) as a standoff analyzer in space missions for airless bodies. *Int. J. Mass Spectrom.* **2012**, *323*, 63–67. [CrossRef]
8. Neuland, M.B.; Grimaudo, V.; Mezger, K.; Moreno-Garcia, P.; Riedo, A.; Tulej, M.; Wurz, P. Quantitative measurement of the chemical composition of geological standards with a miniature laser ablation/ionization mass spectrometer designed for in situ application in space research. *Meas. Sci. Technol.* **2016**, *27*, 035904. [CrossRef]
9. Azov, V.A.; Mueller, L.; Makarov, A.A. Laser ionization mass spectrometry at 55: Quo Vadis? *Mass Spectrom. Rev.* **2022**, *41*, 100–151. [CrossRef] [PubMed]
10. Rohner, U.; Whitby, J.A.; Wurz, P.; Barabash, S. Highly miniaturized laser ablation time-of-flight mass spectrometer for a planetary rover. *Rev. Sci. Instrum.* **2004**, *75*, 1314–1322. [CrossRef]
11. Rohner, U.; Whitby, J.A.; Wurz, P. A miniature laser ablation time-of-flight mass spectrometer for in situ planetary exploration. *Meas. Sci. Technol.* **2003**, *14*, 2159. [CrossRef]
12. Galimov, E. Phobos sample return mission: Scientific substantiation. *Sol. Syst. Res.* **2010**, *44*, 5–14. [CrossRef]
13. Wurz, P.; Bandy, T.; Mandli, P.; Studer, S.; Havoz, S.; Blaukovitsch, M.; Plet, B.G.; Tulej, M.; Piazza, D.; Schmidt, P.K. In Situ Lunar Regolith Analysis by Laser-Based Mass Spectrometry. In Proceedings of the 2023 IEEE Aerospace Conference, Big Sky, MT, USA, 4–11 March 2023; pp. 1–10.
14. Lin, Y.; Yu, Q.; Hang, W.; Huang, B. Progress of laser ionization mass spectrometry for elemental analysis—A review of the past decade. *Spectrochim. Acta Part B At. Spectrosc.* **2010**, *65*, 871–883. [CrossRef]
15. Brinckerhoff, W.; Managadze, G.; McEntire, R.; Cheng, A.; Green, W. Laser time-of-flight mass spectrometry for space. *Rev. Sci. Instrum.* **2000**, *71*, 536–545. [CrossRef]
16. Zayhowski, J.J. Passively Q-switched Nd: YAG microchip lasers and applications. *J. Alloys Compd.* **2000**, *303*, 393–400. [CrossRef]
17. Bhandari, R.; Taira, T. Megawatt level UV output from [110] Cr4+: YAG passively Q-switched microchip laser. *Opt. Express* **2011**, *19*, 22510–22514. [CrossRef]
18. Zayhowski, J.J.; Dill, C. Diode-pumped passively Q-switched picosecond microchip lasers. *Opt. Lett.* **1994**, *19*, 1427–1429. [CrossRef]
19. Wang, P.; Zhou, S.-H.; Lee, K.; Chen, Y. Picosecond laser pulse generation in a monolithic self-Q-switched solid-state laser. *Opt. Commun.* **1995**, *114*, 439–441. [CrossRef]
20. Braun, B.; Kärtner, F.; Zhang, G.; Moser, M.; Keller, U. 56-ps passively Q-switched diode-pumped microchip laser. *Opt. Lett.* **1997**, *22*, 381–383. [CrossRef]
21. Li, C.-y.; Dong, J. Pump beam waist-dependent pulse energy generation in Nd: YAG/Cr^{4+}: YAG passively Q-switched microchip laser. *J. Mod. Opt.* **2016**, *63*, 1323–1330. [CrossRef]
22. Chumikov, A.; Cheptsov, V.; Wurz, P.; Lasi, D.; Jost, J.; Managadze, N. Design, characteristics and scientific tasks of the LASMA-LR laser ionization mass spectrometer onboard Luna-25 and Luna-27 space missions. *Int. J. Mass Spectrom.* **2021**, *469*, 116676. [CrossRef]
23. Riedo, A.; Neuland, M.; Meyer, S.; Tulej, M.; Wurz, P. Coupling of LMS with a fs-laser ablation ion source: Elemental and isotope composition measurements. *J. Anal. At. Spectrom.* **2013**, *28*, 1256–1269. [CrossRef]

24. Schaper, W.; Rudnik, K.; Steininger-Fetzer, M. Pulse current sources for high power laser application. In Proceedings of the 8th European Space Power Conference, Constance, Germany, 14–19 September 2008; p. 17.
25. Andreoni, E.; Xu, J.; Cartaleva, S.; Celli, R.; Mango, F.; Gozzini, S. A simple system of thermal control and frequency stabilization of solitary diode lasers. *Rev. Sci. Instrum.* **2000**, *71*, 3648–3652. [CrossRef]